Framework for Statistical Parametric Mapping of the Interactions between Glioblastoma Location, Treatment, Prognostic Variables, and Survival Using a Phase III Trial

Francesco Sanvito[1,2], Catalina Raymond[1,2], Donatello Telesca[3], Jingwen Yao[1,2], Lauren E. Abrey[4], Josep Garcia[5], Brian Simmons[5], Olivier Chinot[6], Frank Saran[7], Ryo Nishikawa[8], Roger Henriksson[9], Warren P. Mason[10], Wolfgang Wick[11], Timothy F. Cloughesy[12], and Benjamin M. Ellingson[1,2]

Downloaded from aacrjournals.org/clincancerres/article-pdf/32/11/2230/3796381/ccr-25-4419.pdf by DKFZ - German Cancer Research Center, m.krumbach@dkfz.de on 28 October 2026

ABSTRACT

Purpose: Brain tumor location is known to affect survival, but there is a lack of methodologic tools for systematically studying the complex interplay between brain tumor location, prognostic variables, treatment schemes, and survival.

Experimental Design: A total of 592 prospectively enrolled patients with newly diagnosed glioblastoma from the phase III AVAglio trial, randomized to postsurgical chemoradiation with or without bevacizumab, were retrospectively analyzed. Statistical parametric mapping was conducted with multivariate Cox proportional hazards models at the voxel-wise level, incorporating dedicated interaction variables to evaluate the impact of baseline tumor volume and treatment arm on survival for different tumor locations from magnetic resonance imaging (MRI) scans, with subsequent cluster-based correction for multiple testing and mathematical estimation of regional survival curves.

Results: Tumor location in the right prefrontal cortex was an independent favorable prognostic factor [median hazard ratio (HR) = 0.57] for survival, whereas tumor involvement in left hemisphere eloquent areas with language and visual functions was unfavorable (median HR = 1.69). Larger presurgical tumor volumes were associated with shorter survival independent of tumor location (HR = 1.005), but the effect was larger for tumor locations including eloquent structures (HR ranging 1.008–1.015), whereas nonsignificant for anterior frontal locations. Bevacizumab seemed to grant a survival benefit when specific brain regions were involved or spared by the tumor, but this result was not confirmed after correction for multiple testing.

Conclusions: This workflow allows to map the survival effects of variables onto specific brain tumor locations, revealing location dependency of prognostic variables such as tumor volume, and potentially of treatment schemes, with relevant implications in risk stratification and clinical management.

Introduction

Glioblastoma (GBM) is the most common primary malignant brain tumor (1) and has a poor prognosis despite intensive standard treatment of surgical resection and adjuvant chemoradiation, with a median overall survival (OS) ranging from 8 to 16 months across cohorts, as reported in the general population (1) and in clinical trials (2–4). Extensive research efforts are dedicated to developing novel therapeutics and treatment strategies, with more than 250 trials worldwide (5), exploring therapies including immunotherapy, targeted therapy, gene therapy, and various combination regimens. Given the complexity of GBM and the diversity in patient medical histories, it is crucial to develop robust prognostication models, both for clinical management and for identifying responsive cohorts in clinical trials.

The brain is a unique organ in terms of complexity and distribution of functions. Since the early work by Paul Pierre Broca in the 19th century (6), extensive evidence has demonstrated the concept of functional localization within specific brain regions, which has more recently been corroborated by the noninvasive mapping of neurocognitive deficits corresponding to specific stroke or tumor locations, using voxel-wise lesion–symptom mapping (7–9). In brain tumors, lesion location has been shown to be closely linked to functional impairment (9, 10) and psychologic changes (11, 12), with tumors involving eloquent areas known to be responsible for language, motor function, sensation, and visual function showing the largest measurable functional changes after surgery or tumor growth (13, 14).

In addition to the influence on resulting brain function, tumor location has also been linked to different brain tumor biological features. As in breast tumors (15, 16), lung cancers (17, 18), and meningiomas (19, 20) with different genetic alterations showing

[1]UCLA Brain Tumor Imaging Laboratory, Department of Radiological Sciences, David Geffen School of Medicine, University of California Los Angeles, Los Angeles, California. [2]Department of Radiological Sciences, David Geffen School of Medicine, University of California Los Angeles, Los Angeles, California. [3]Department of Biostatistics, University of California, Los Angeles, California. [4]F. Hoffmann-La Roche, Ltd, Basel, Switzerland. [5]Genentech, South San Francisco, California. [6]Aix-Marseille University, AP-HM, Service de Neuro-Oncologie, CHU Timone, Marseille, France. [7]The Royal Marsden NHS Foundation Trust, Sutton, United Kingdom. [8]Saitama Medical University, Saitama, Japan. [9]Department of Radiation Sciences and Oncology, University of Umea, Umea, Sweden. [10]Princess Margaret Hospital, Toronto, Canada. [11]Neurology, University Clinic Heidelberg, Heidelberg University and German Cancer Consortium (DKTK) and CCU Neurooncology, German Cancer Research Center, Heidelberg, Germany. [12]UCLA Neuro-Oncology Program, David Geffen School of Medicine, University of California Los Angeles, Los Angeles, California.

Corresponding Author: Benjamin M. Ellingson, Department of Radiological Sciences, University of California, Los Angeles, 924 Westwood Boulevard, Los Angeles, CA 90024. E-mail: bellingson@mednet.ucla.edu

Clin Cancer Res 2026;32:2230–42

doi: 10.1158/1078-0432.CCR-25-4419

This open access article is distributed under the Creative Commons Attribution-NonCommercial-NoDerivatives 4.0 International (CC BY-NC-ND 4.0) license.

©2026 The Authors; Published by the American Association for Cancer Research

Translational Relevance

Glioblastoma location is closely linked to neurologic function, tumor biology, surgical resectability, and, ultimately, patient survival. Here, we provide a robust framework to implement a data-driven unbiased methodology to map the survival impact of prognostic variables and treatment regimens onto different brain tumor locations. This novel and versatile tool can be used for the combined analysis of clinical and imaging datasets in clinical trials to test new hypotheses on the differential importance of prognostic variables for different brain tumor locations, as well as differential treatment efficacy. For robustness, we also illustrate how to incorporate corrections for multiple testing, as well as a mathematical approach to visualize regional survival probability curves. As a paradigmatic example on a large clinical trial cohort, we demonstrate how tumor location modulates the impact of tumor volume on survival. This statistical tool has the potential to improve prognostication and location-based treatment choices in the future.

preferential anatomic distributions, evidence suggests that primary brain tumors also exhibit a preferential localization depending on clinically relevant genetic and epigenetic signatures, including H3K27M-mutant diffuse midline gliomas (21), isocitrate dehydrogenase (IDH)–mutant gliomas (22, 23), EGFR-altered GBMs (23, 24), and PDGFRA-amplified GBMs (24). Additionally, metastatic brain tumors with differing primary pathologies also seem to have a distinct and preferred neuroanatomic distribution (25, 26).

Despite the critical relevance of tumor location, which not only is linked to neurologic function and tumor molecular signatures but also directly associated with patient survival (27–39), the current methodologic tools to investigate its role exhibit two main limitations. First, previous studies evaluating GBM location in survival analyses have mainly adopted investigator-dependent general categorizations of tumor sites according to the cerebral lobe involved (28, 30, 33), and/or laterality (31, 38), and/or location depth (27, 37), which are inherently approximative and introduce inconsistencies across studies. Second, and most importantly, there is a lack of methodology for systematically studying the complex interplay between tumor location within the brain, genetic and prognostic variables, treatment response, and the impact on survival.

In the current study, we present a framework for studying the influence of tumor location on survival with an unbiased investigator-independent approach while interrogating its interplay with prognostic variables and experimental treatment. Building on the concept of statistical parametric mapping (SPM; ref. 40), which conducts statistical tests at the voxel-wise level (23), we developed a methodology based on multivariate Cox regression statistical parameter mapping (SPM) at the voxel-wise level, similar to what other studies have proposed for Alzheimer disease (41), lung cancer (42), and substance abuse (43). Most importantly, we integrate the use of dedicated interaction terms, as well as a rigorous approach for multiple testing correction and for the modeling of regional survival curves associated with tumor locations in specific brain regions. By showcasing this framework in datasets from a large, multicenter, international phase III trial testing chemoradiation with or without bevacizumab in newly diagnosed GBM (ClinicalTrials.gov #NCT00943826; ref. 3), we demonstrate how this approach can be used to integrate the anatomic location of brain tumor involvement into the interpretation of the overall impact of experimental treatments and prognostic variables on patient survival.

Materials and Methods

Clinical trial source

Clinical information and imaging datasets from patients with pathologically confirmed, newly diagnosed supratentorial GBM enrolled in a prospective multicenter phase III clinical trial (AVAglio, ClinicalTrials.gov #NCT00943826; ref. 3) were retrospectively reviewed. In this clinical trial, all patients were treated with postsurgical concurrent radiotherapy and temozolomide followed by adjuvant temozolomide according to the Stupp protocol (2). Patients were randomized (1:1), with a double-blinded design, to receive either placebo or bevacizumab starting during concomitant chemoradiation and until disease progression or unacceptable toxicity. Inclusion criteria for the present retrospective study were as follows: availability of postsurgical magnetic resonance imaging (MRI) images, O^6-methylguanine-DNA methyltransferase (MGMT) methylation status from histopathology, and survival data. The sample size for this retrospective analysis was determined by including all patients meeting these criteria; therefore, no power analysis was performed. All patients gave written informed consent to participate in the original AVAglio clinical trial (ClinicalTrials.gov #NCT00943826), which adhered to the principles of the Declaration of Helsinki.

MRI analysis

Postsurgical images were acquired as part of a standardized protocol (44). T_2-weighted (T_2w), T_2w fluid-attenuated inversion recovery (T_2w-FLAIR), and pre- and postcontrast T_1-weighted images were registered to the reference Montreal Neurological Institute (MNI) atlas and simultaneously resampled to 1-mm isotropic voxels, using the FMRIB Software Library (FSL, www.fsl.fmrib.ox.ac.uk, RRID: SCR_002823) built-in *flirt* function (12 degrees of freedom, mutual information algorithm, and trilinear interpolation), as previously described (23). A previously described semi-automated thresholding method (45) was used to obtain one segmentation of the contrast-enhancing tumor and another whole-tumor segmentation combining enhancing and nonenhancing T_2-FLAIR hyperintense tumor, necrotic regions, and the surgical cavity. The whole-tumor segmentation (including the surgical cavity) represented the approximate extent and location of the presurgical tumor. The segmentations were performed by trained lab members and refined by a staff neuroradiologist (45). Readers curating the segmentations were blinded to clinical data, treatment arm, and OS.

Statistical models

Multivariate Cox proportional hazards models were used to study the association between several covariates and OS, first with models independent of tumor locations (models 1–2, non-voxel-wise) and then with voxel-wise models mapping the impact of different covariates for each brain region (SPM; model 3–6). Cox models were run using the MATLAB (R2021b Update 6, RRID: SCR 001622) *coxphfit* function. For all models, all values (x) of the covariates (including both continuous and binary variables, for both voxel-wise and non–voxel-wise models) of each subject j were centralized to their mean value ($\bar{x}$) across the cohort: $x_j - \bar{x}$. The overall integrated framework (**Fig. 1**) for voxel-wise models includes the analysis of tumor presence at each voxel, the adjustment for

Downloaded from aacrjournals.org/clincancerres/article-pdf/32/11/2230/3796381/ccr-25-4419.pdf by DKFZ - German Cancer Research Center, m.krumbach@dkfz.de on 28 October 2026

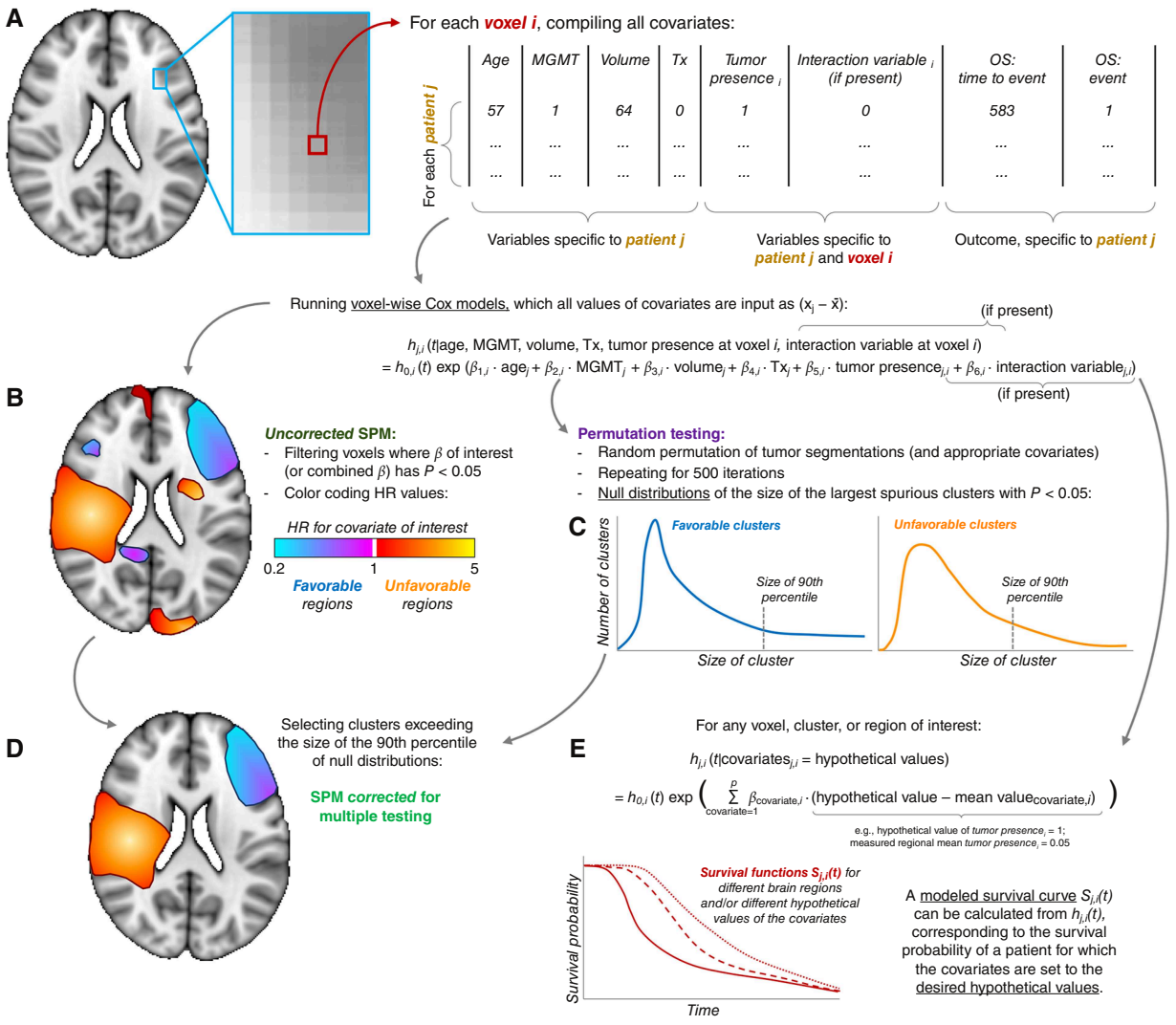


Figure 1.

Workflow for SPM with voxel-wise multivariate Cox models. Voxel-wise multivariate models were run by including voxel-specific covariates (**A**), and the HR for the effect coefficient of the covariate of interest was mapped voxel-wise to visualize the uncorrected SPM (**B**). Permutation testing was used for multiple testing correction (**C**) to select the clusters more likely to represent true-positive results (**D**). Modeled survival curves were calculated using the regional effect coefficients estimated by the models by imposing the desired hypothetical values of the covariates of interest (**E**).

other covariates, a methodology to test interaction terms, multiple comparison correction through permutation testing, and a mathematical modeling of regional survival curves.

Non–voxel-wise models

First, a standard non–voxel-wise model with four covariates was run to assess the overall impact of age, MGMT promoter methylation status, baseline tumor volume, and treatment independent of tumor location (model 1, Eq. A):

$$h_j(t|Age,\ MGMT,\ Volume,\ Tx) = h_0(t)\exp\left(\beta_1 \cdot Age_j + \beta_2 \cdot MGMT_j + \beta_3 \cdot Volume_j + \beta_4 \cdot Tx_j\right) \quad \text{(A)}$$

Age was measured in years. MGMT promoter methylation status was coded as 1 for methylated and 0 for unmethylated. Baseline tumor volume was obtained from the segmentations and measured in cc. Treatment (Tx) was coded as 1 for chemoradiation + bevacizumab and 0 for chemoradiation + placebo.

An additional non–voxel-wise model was run by adding an interaction variable to assess the interplay between baseline volume and treatment (5 covariates; model 2, Eq. B):

$$h_j(t|Age,\ MGMT,\ Volume,\ Tx,\ Volume \cdot Tx) = h_0(t)\exp\left(\beta_1 \cdot Age_j + \beta_2 \cdot MGMT_j + \beta_3 \cdot Volume_j + \beta_4 \cdot Tx_j + \beta_5 \cdot Volume_j \cdot Tx_j\right) \quad \text{(B)}$$

In this model, $\beta_4 + V \times \beta_5$ represents the effect coefficient of treatment given a certain volume V (coefficient of $Tx \mid volume = V$); $\beta_3 + \beta_5$ represents the coefficient of volume in case of treatment with chemoradiation + bevacizumab (coefficient of $volume \mid Tx = 1$); and

Downloaded from aacrjournals.org/clincancerres/article-pdf/32/11/2230/3796381/ccr-25-4419.pdf by DKFZ - German Cancer Research Center, m.krumbach@dkfz.de on 28 October 2026

β_3 represents the coefficient of volume in case of treatment with chemoradiation + placebo (coefficient of *volume* | $Tx = 0$). The P values for combined coefficients can be calculated by adapting the procedure described by Rosner (Supplementary Appendix S1; ref. 46).

Voxel-wise model with tumor location

To include information about tumor location, we built a multivariate model (model 3, with no interaction terms) that includes the binary presence or absence of the tumor in each voxel i (*tumor presence*) for each patient j (model 3, Eq. C):

$$h_{j,i}(t|Age,\ MGMT,\ Volume,\ Tx,\ Tumor\ Presence\ at\ voxel\ i) = h_{0,i}(t)\exp\Big(\beta_{1,i}\cdot Age_j + \beta_{2,i}\cdot MGMT_j + \beta_{3,i}\cdot Volume_j + \beta_{4,i}\cdot Tx_j + \beta_{5,i}\cdot Tumor\ Presence_{j,i}\Big) \quad (C)$$

This model was run voxel-wise (i.e., for each image voxel " i " of the reference MNI space, **Fig. 1A**). The tumor presence in a specific voxel i was obtained from the segmentations registered to the reference MNI space and coded as 1 for tumor presence and 0 for tumor absence. Only voxels where tumor was present in at least 1% of the cohort were included in this analysis (Supplementary Fig. S1). Voxel-wise parametric maps of P values and hazard ratios (HR) for $\beta_{5,i}$ were obtained, representing whether the tumor localization in a certain voxel (*tumor presence* in voxel i) was a predictor of OS after adjusting for the other covariates.

Voxel-wise model with interaction of tumor presence and tumor volume

To study the interplay between tumor location and baseline tumor volume, we expanded the voxel-wise model to include a dedicated interaction term (model 4, with 6 covariates including the interaction term; Eq. D):

$$h_{j,i}(t|Age,\ MGMT,\ Volume,\ Tx,\ Tumor\ Presence\ at\ voxel\ i,\ Volume\cdot Tumor\ Presence\ at\ voxel\ i) = h_0(t)\exp\Big(\beta_{1,i}\cdot Age_j + \beta_{2,i}\cdot MGMT_j + \beta_{3,i}\cdot Volume_j + \beta_{4,i}\cdot Tx_j + \beta_{5,i}\cdot Tumor\ Presence_{j,i} + \beta_{6,i}\cdot Volume_j\cdot Tumor\ Presence_{j,i}\Big) \quad (D)$$

The interaction term was included in the model run in each voxel (**Fig. 1A**). In this model, the combined coefficient $\beta_{3,i} + \beta_{6,i}$ represents the effect for baseline volume in voxels where tumor is present (coefficient of *volume* | *tumor presence*; combined P value calculation in Supplementary Appendix S1).

Voxel-wise model with interaction of tumor presence and treatment

An alternative voxel-wise model was employed to evaluate the interplay between tumor location and treatment by including the dedicated interaction term (model 5, with 6 covariates including the interaction term; Eq. E):

$$h_{j,i}(t|Age,\ MGMT\ status,\ Volume,\ Tx,\ Tumor\ Presence\ at\ voxel\ i,\ Tx\cdot Tumor\ Presence\ at\ voxel\ i) = h_0(t)\exp\Big(\beta_{1,i}\cdot Age_j + \beta_{2,i}\cdot MGMT_j + \beta_{3,i}\cdot Volume_j + \beta_{4,i}\cdot Tx_j + \beta_{5,i}\cdot Tumor\ Presence_{j,i} + \beta_{6,i}\cdot Tx_j\cdot Tumor\ Presence_{j,i}\Big) \quad (E)$$

In this model, the combined coefficient $\beta_{4,i} + \beta_{6,i}$ corresponds to the effect of the bevacizumab treatment arm in case of tumor presence in voxel i (coefficient of Tx | *tumor presence*—i.e., the effect of Tx when *tumor presence*$_i = 1$; combined P value calculation in Supplementary Appendix 1). Additionally, the coefficient $\beta_{4,i}$ corresponds to the effect of bevacizumab experimental treatment in case of tumor absence in voxel i (coefficient of Tx | *tumor absence*—i.e., the effect of Tx when *tumor presence*$_i = 0$). As $\beta_{6,i}$ in this model can yield extreme effect coefficients for the interaction term in voxels where $Tx \times$ *tumor presence* is equal to zero in most patients, only voxels where Tx $\times$ *tumor presence* equals 1 in at least 1% of patients are included in this analysis.

Sensitivity analysis

Finally, a comprehensive voxel-wise model with both interaction terms for tumor presence and volume and for tumor presence and treatment was run (model 6, with 7 covariates including 2 interaction terms) as a sensitivity analysis to verify the robustness of interaction terms.

Uncorrected parametric brain maps

For each effect coefficient of interest $\beta_{covariate,i}$ (including combined coefficients, e.g., $\beta_{4,i}$+$\beta_{6,i}$), a voxel-wise map of HR was calculated as $\exp(\beta_{covariate,i})$. This map was filtered to include only voxels where $P < 0.05$ for $\beta_{covariate}$. Then, the built-in FSL function *fsl-cluster* was used to separate different clusters and to exclude clusters with size <1 cc (**Fig. 1B**).

Correction for multiple testing using random permutations

An inherent issue of SPM is the presence of false-positive statistical results due to multiple testing. With a number of statistical tests in the order of 10^6, traditional multiple comparison corrections such as the Bonferroni correction are not ideal, both due to type II errors and due to their dependency on image resolution, as reducing voxel size exponentially increases the number of statistical tests (47). Here, we implemented an approach based on size-based cluster correction following permutation testing (48). A dedicated set of 500 permutations was run for each of these four uncorrected voxel-wise maps of interest: *tumor presence* from model 3, *volume* | *tumor presence* from model 4, Tx | *tumor presence* from model 5, and Tx | *tumor absence* from model 5. Permutations were performed by randomizing the association between the covariate of interest and OS, while maintaining the associations between the other covariates and OS, maintaining the interaction variables consistent (when present), and consistently adjusting for tumor size, as recommended for voxel-wise analyses (47). For each dedicated set of 500 permutations, null distributions of the volumes of the 500 largest favorable ($\beta < 0$, $P < 0.05$) and unfavorable ($\beta > 0$, $P < 0.05$) false-positive clusters were analyzed separately (**Fig. 1C**). In the uncorrected voxel-wise map from the original nonpermutated model, favorable and unfavorable clusters were considered true positive (i.e., surviving multiple comparison correction) if their volume exceeded the 90th percentile of the distribution of volumes of false-positive favorable and unfavorable clusters, respectively, and therefore included in the corrected voxel-wise maps (**Fig. 1D**). The multiple comparison approach is described in more detail in Supplementary Appendix S2.

Modeling of regional survival curves

As all covariates were treated as continuous variables and centered to the cohort mean value ($x_j - \bar{x}$), the baseline hazard function

Downloaded from aacrjournals.org/clincancerres/article-pdf/32/11/2230/3796381/ccr-25-4419.pdf by DKFZ - German Cancer Research Center, m.krumbach@dkfz.de on 28 October 2026

$h_0(t)$ and corresponding baseline survival function $S_0(t)$ of all models had two valuable properties. First, $h_0(t)$ and $S_0(t)$ correspond to a theoretical patient with mean values of all covariates; therefore, the modeled $S_0(t)$ overlaps completely with the observed survival curve of the cohort (Supplementary Figure S2A). Although a patient with a "mean value" of dichotomous variables (e.g., treatment arm = 0.4949) does not exist in the real world, treating these variables as continuous covariates guarantees the necessary mathematical properties of $h_0(t)$ and $S_0(t)$. Second, calculating $h_0(t)$ and $S_0(t)$ in this way also allows stability during the introduction of any additional covariates (including *tumor presence* and interaction variables). Therefore, $h_0(t)$ and $S_0(t)$ are the same in all models and in all voxels (Supplementary Figure S2), and $h_{0,Model1}(t)$ can be used to calculate the hazard function $h_{j,i}(t)$ for tumor involvement in voxel i in all voxel-wise models, without the need of extracting all voxel-specific $h_{0,i}(t)$ functions, which would be challenging from a computational standpoint and unnecessary.

In model *3*, the voxel-specific hazard function $h_{j,i}(t)$ for a patient with tumor presence in voxel i (and with all other covariates set to the mean value of the cohort) can be calculated from Eq. C using $h_{0,Model1}(t)$, the voxel-specific coefficient for tumor presence ($\beta_{5,i}$), the desired hypothetical value of tumor presence (*tumor presence* = 1), and the measured mean value of *tumor presence* in voxel i across patients (corresponding to the tumor frequency in the voxel, as in Supplementary Fig. S1):

$$h_{j,i}\left(t|\overline{Age},\ \overline{MGMT},\overline{Volume},\ \overline{Tx},\ Tumor\ Presence_{j,i}=1\right) = h_{0,Model1}(t)\exp\left[\beta_{5,i}\cdot\left(1-\overline{Tumor\ Presence_i}\right)\right] \quad \text{(F)}$$

where the overbar on a variable term denotes the mean value of the variable across the cohort (e.g., $\overline{x}$ to denote the mean of all x_j values).

In model 4, the presence of an interaction variable adds a degree of complexity for the voxel-specific hazard function $h_{j,i}(t)$, as it requires the extraction of regional $\beta_{covariate,i}$ coefficients for the volume covariate and for the interaction term, as well as the measured voxel-wise mean of tumor presence (*tumor presence*$_i$ with overbar) and voxel-wise mean of the interaction term across patients (*volume* × *tumor presence*$_i$ with overbar). The hazard function $h_{j,i}(t)$ for a patient with a tumor of a certain hypothetical volume (V_{hyp}) involving voxel i (and all other covariates set to the mean value of the cohort) can be calculated from Eq. D and written as

$$\begin{aligned} h_{j,i}\Big(t|\overline{Age},\ \overline{MGMT},\ Volume_j=V_{hyp},\ \overline{Tx},\ Tumor\ Presence_{j,i}=1,\\ Volume_j\cdot Tumor\ Presence_{j,i}=V_{hyp}\cdot 1\Big)\\ = h_{0,Model1}(t)\exp\Big[\beta_{3,i}\cdot\left(V_{hyp}-\overline{Volume}\right)\\ +\beta_{5,i}\cdot\left(1-\overline{Tumor\ Presence_i}\right)\\ +\beta_{6,i}\cdot\left[\left(V_{hyp}\cdot 1\right)-\overline{(Volume\cdot Tumor\ Presence_i)}\right]\Big] \end{aligned} \quad \text{(G)}$$

In model 5, similarly, a voxel-specific hazard function $h_{j,i}(t)$ can be calculated from Eq. E using the desired hypothetical values of treatment arm (Tx_{hyp} = 1 to model the hazard function for bevacizumab; Tx_{hyp} = 0 for placebo) and tumor presence (*tumor presence*$_{hyp}$ = 1 to model the hazard function for tumor presence in the voxel; *tumor presence*$_{hyp}$ = 0 for tumor absence), as well as the voxel-specific coefficients $\beta_{covariate,i}$, and the voxel-specific mean of tumor presence (*tumor presence*$_i$ with overbar) and interaction term (*Tx* × *tumor presence*$_i$ with overbar):

$$\begin{aligned} h_{j,i}\Big(t|\overline{Age},\ \overline{MGMT},\ \overline{Volume},\ Tx_j=Tx_{hyp},\ Tumor\ Presence_{j,i}\\ = Tumor\ Presence_{hyp},\ Tx_j\cdot Tumor\ Presence_{j,i}\\ = Tx_{hyp}\cdot Tumor\ Presence_{hyp}\Big) = h_{0,Model1}(t)\exp\Big[\beta_{4,i}\cdot\left(Tx_{hyp}-\overline{Tx}\right)\\ +\beta_{5,i}\cdot\left(Tumor\ Presence_{hyp}-\overline{Tumor\ Presence_i}\right)\\ +\beta_{6,i}\cdot\left[\left(Tx_{hyp}\cdot\ Tumor\ Presence_{hyp}\right)-\overline{(Tx\cdot Tumor\ Presence_i)}\right]\Big] \end{aligned} \quad \text{(H)}$$

Once the voxel-specific hazard function $h_{j,i}(t)$ is obtained, the corresponding voxel-specific survival function $S_{j,i}(t)$ can be calculated as the exponential of the negative cumulative sum of $h_{j,i}(t)$, as in any traditional Cox model. Given that survival functions corresponding to a single voxel may be of limited value, larger brain regions can be analyzed by extracting regional median coefficients $\beta_{covariate,region}$ and regional median values of mean voxel-wise variables (i.e., the terms with the overbars), and then the regional survival function $S_{j,region}(t)$ from the regional hazard function $h_{j,region}(t)$ is calculated. The calculation of regional survival curves is described in more detail in Supplementary Appendix S3; the curve plots were obtained using the Python (version 3.10.10) *matplotlib* library (RRID: SCR_008624).

Results

Patient characteristics

A total of 592 patients from the original AVAglio trial (3) met the inclusion criteria for this retrospective analysis. The median OS for all patients in the trial was 536 days. Death was observed in 513 (86.66%) patients, whereas 79 (13.34%) patients were alive at the end of the study and were considered censored for survival analysis. Age at the time of MRI data collection was 55.85 ± 10.66 years [mean ± standard deviation (SD)], and tumor volume at baseline measured on MRI was 66.91 ± 52.41 cc. A total of 201 (33.95%) patients were diagnosed with GBM bearing MGMT promoter methylation and 391 (66.05%) patients without methylation. A total of 293 (49.49%) patients in the study received chemoradiation + bevacizumab, and 299 (50.51%) patients were assigned to the control group receiving chemoradiation + placebo. All tumors were supratentorial, with higher frequency in the subcortical and periventricular white matter and with right-hemispheric lesions slightly more prevalent than left-sided lesions (Supplementary Fig. S1).

Predictors of survival, not accounting for tumor location

As a first simple analysis, we evaluated the association between baseline variables and survival using a standard non–voxel-wise Cox model without tumor location or interaction terms (model 1). As expected, an older age ($P < 0.0001$; HR = 1.02) and a larger baseline tumor volume ($P < 0.0001$; HR = 1.005) were significant prognostic factors for shorter OS, whereas MGMT promoter methylation ($P < 0.0001$; HR = 0.41) was predictive of longer OS (**Table 1**), likely due to the survival benefit associated with temozolomide in methylated tumors (49). No significant association between the treatment (Tx) group (chemoradiation with or without bevacizumab) and OS was seen ($P = 0.083$, HR = 0.86), consistent with previous reports from the original clinical trial (3). Notably, other prognostic variables may be potentially evaluated, such as Karnofsky Performance Status (KPS). In this cohort, KPS was not an independent predictor factor in multivariate analysis, likely due to

Downloaded from aacrjournals.org/clincancerres/article-pdf/32/11/2230/3796381/ccr-25-4419.pdf by DKFZ - German Cancer Research Center, m.krumbach@dkfz.de on 28 October 2026

Table 1. Survival analysis not accounting for tumor location (non–voxel-wise models).

Variable coefficient	Interpretation	Variable coding	*P* value	HR
β_1 in model 1	Age	Years	<0.0001	1.02
β_2 in model 1	MGMT status	1 = methylated; 0 = unmethylated	<0.0001	0.41
β_3 in model 1	Volume	cc	<0.0001	1.005
β_4 in model 1	*Tx*	1 = ChemoRT + Bev; 0 = ChemoRT + placebo	0.083	0.86
$\beta_4 + V \times \beta_5$ in model 2	*Tx* | *volume* = V	Tx: 1 = ChemoRT + Bev; Tx: 0 = ChemoRT + placebo Volume: V in cc	0.19 for any 0 cc < V < 100 cc	0.83×1.0004^V
$\beta_3 + \beta_5$ in model 2	*Volume* | *Tx* = 1	Volume in cc Tx: 1 = ChemoRT + Bev	<0.0001	1.005
β_3 in model 2	*Volume* | *Tx* = 0	Volume in cc Tx: 0 = ChemoRT + placebo	<0.001	1.005

Abbreviations: β, effect coefficient of the Cox models; Bev, bevacizumab; cc, cubic centimeters; ChemoRT, chemoradiation.

collinearity with presurgical tumor volume (model 1B, Supplementary Table S1), and was therefore not included in further models.

When expanding the model to introduce an interaction term of baseline volume and treatment arm (model 2), the experimental treatment arm (chemoradiation + bevacizumab) was not associated with an OS benefit for any tumor size (**Table 1**, $P = 0.19$) compared with the control treatment arm (chemoradiation + placebo), suggesting no role for presurgical tumor volume in modulating a treatment-induced survival benefit.

Impact of tumor location on survival with SPM

To achieve an investigator-independent data-driven evaluation of the association between tumor location and OS, we updated the survival model to incorporate a voxel-wise variable coding for *tumor presence* (model 3). After cluster-based correction for multiple testing, *tumor presence* was an independent predictor of OS in brain regions corresponding to two different clusters. Tumor involvement in the favorable cluster I was associated with longer OS (violet-blue in **Fig. 2A** and **B**; median HR = 0.57; histograms in **Fig. 2C**) compared with no tumor involvement in cluster I. Cluster I mainly included brain regions with associative functions, such as the cortical and juxtacortical areas of the right superior and middle frontal gyri as well as the centrum semiovale in the right frontal lobe (violet-blue in **Fig. 2A** and **B**). Compared with eloquent regions, tumors in associative regions may safely receive a more radical surgical resection, which is associated with longer survival (28, 32, 37–39, 50, 51), and are less likely to cause an abrupt impairment in neurologic and clinical functions, which is also linked to shorter survival (28, 37, 39, 52, 53), as also supported by previous reports on frontal tumors bearing longer survival compared with deep-seated and surgically unfavorable locations (27, 28, 31, 32, 37, 39, 54). In line with this interpretation, we also found that tumor presence was associated with shorter OS in several regions with eloquent functions and deep-seated areas, included in the unfavorable cluster II (red-yellow in **Fig. 2A** and **B**; median HR = 1.69,; histograms in **Fig. 2C**), where tumor growth and invasion likely affected neurologic and clinical functions and compromised the feasibility of a safe resection. In more detail, cluster II (red–yellow in **Fig. 2A** and **B**) included eloquent regions such as the basal and medial occipitotemporal regions (which serve visual processing functions), large portions of the posterior and posterolateral temporal lobe and white matter areas belonging to the arcuate fasciculus (regions involved in auditory and language processing), and deep-seated regions such as the splenium of the corpus callosum, the left thalamus, and left parahippocampal gyrus. These findings show a remarkable concordance with previous reports from voxel-wise analyses, which highlighted an association between poor prognosis and tumor locations in deep-seated brain structures (corpus callosum and basal ganglia) or in left-hemisphere eloquent regions (territories belonging to the arcuate fasciculus, the inferior frontooccipital fasciculus, primary and supplementary motor cortices, and parahippocampal gyrus; refs. 52, 55, 56).

The modeling of the regional survival curves allowed the visualization of the survival probability for a hypothetical patient with tumor involvement in these clusters (**Fig. 2D**) or in some representative regions of interest (**Fig. 2E** and **F**; assuming mean values for all other covariates). Based on the regional survival curves, the estimated median OS for patients with tumors involving cluster I was 729 days, and it was 433 days for tumor locations in cluster II (vs. 536 days of observed median OS in the cohort).

Impact of baseline tumor volume on survival for different tumor locations

As presurgical tumor size is associated with OS in untreated GBM, both in the current study ($P < 0.0001$; HR = 1.005; **Table 1**) and in previous independent cohorts (55, 57–60), we explored whether tumor size showed an interplay with the tumor location in survival analysis, under the hypothesis that larger tumors would negatively affect survival predominantly in eloquent and deep-seated regions. To test this hypothesis, we expanded the voxel-wise Cox model to include a dedicated interaction term between *volume* and *tumor presence* (model 4).

After correcting for multiple testing, SPM showed that a larger presurgical tumor volume is an independent unfavorable prognostic factor for OS in tumors involving most areas of the brain, comprised in a single large cluster (cluster III, orange-yellow in **Fig. 3A**) but with variability in regional effect sizes. Notably, the effect size of *volume* in cluster III (median HR = 1.008 and up to HR~1.015, corresponding to a 0.8% and a 1.5% increased risk of death per cc of volume, respectively; histograms in **Fig. 3B**) was significantly larger than the effect size of tumor volume independent of location (HR = 1.005 for volume independent of tumor location in model 1, corresponding to a 0.5% increased risk of death per cc of volume, dashed line in **Fig. 3B**). Additionally, for tumors with involvement in eloquent regions such as the motor and somatosensory areas (e.g., region

Downloaded from aacrjournals.org/clincancerres/article-pdf/32/11/2230/3796381/ccr-25-4419.pdf by DKFZ - German Cancer Research Center, m.krumbach@dkfz.de on 28 October 2026

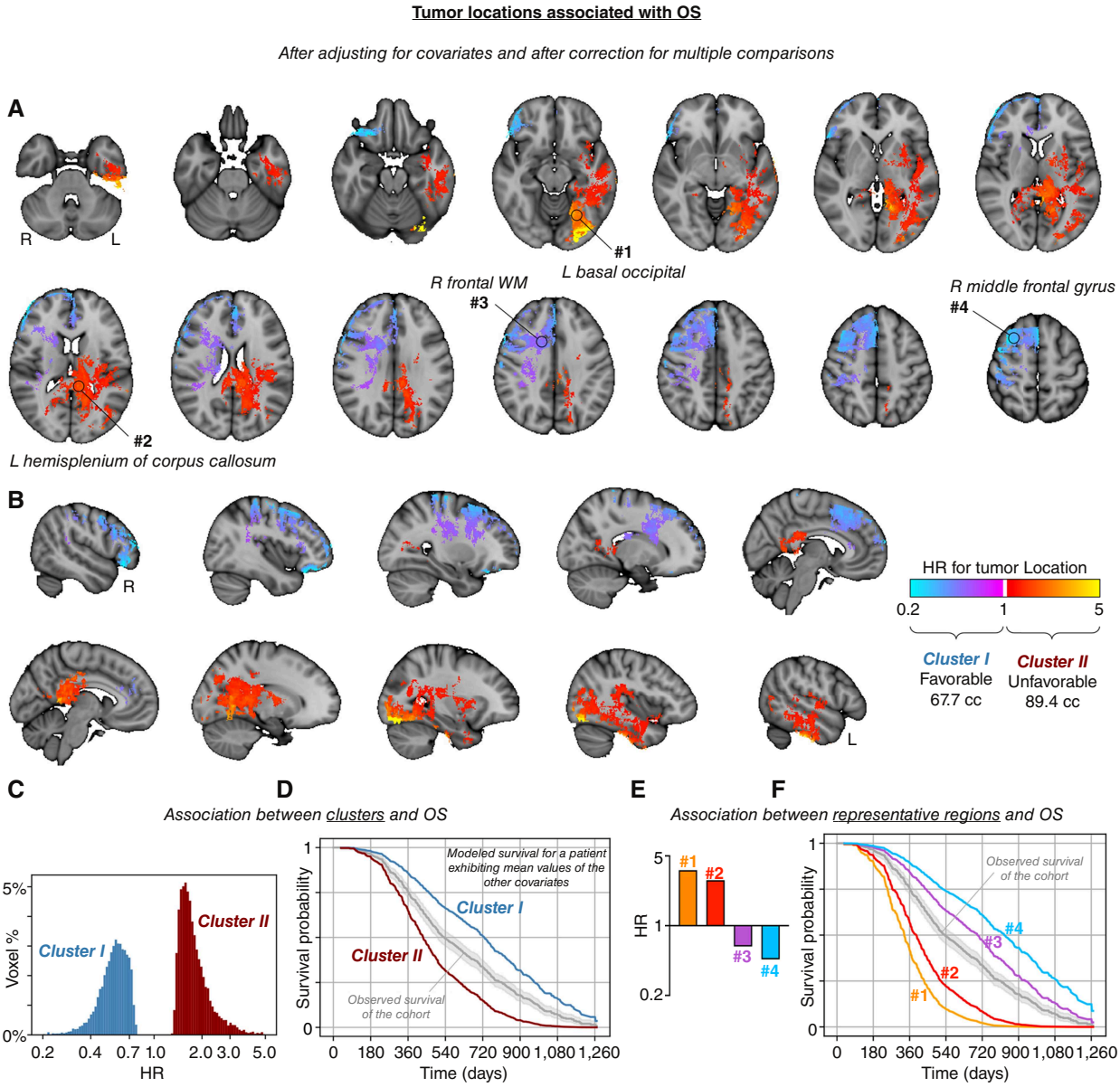


Figure 2.

Impact of voxel-wise tumor location on survival (*tumor presence* in model 3). Anterior right frontal locations are associated with a longer survival (cluster I, violet-blue), whereas numerous other locations in the left hemisphere are associated with a shorter survival (cluster II, red-orange; **A** and **B**, only regions with $P < 0.05$ and surviving multiple testing correction). Prognostic differences can be visualized by plotting HR (**C** and **E**) and displaying modeled survival curves (**D** and **F**) corresponding to the clusters and to specific representative brain regions of interest, respectively. L, left; R, right; WM, white matter.

#1 in **Fig. 3A**), the impact of larger tumor volumes on shorter OS was particularly pronounced (HR = 1.015). Conversely, in regions outside cluster III, the baseline tumor volume was not a significant predictor of OS, and the estimated HR was lower than the HR independent of tumor location (median HR = 1.003, corresponding to a 0.3% increased risk of death per cc of volume, which was not significant, $P > 0.05$, dotted line in **Fig. 3B**). Although baseline tumor size is a prognostic factor independent of tumor location (55, 57–60), these findings highlight that its impact on OS is location dependent, and each additional cc of disease may bear a deeper impact on neurologic functions and surgical resectability when the lesion is located in more sensitive brain regions. This novel finding may also partially explain why some previous articles (28, 34, 61, 62) reported no clear association between baseline pretreatment volume and OS, possibly due to the confounding interplay of tumor locations.

The modeling of regional survival curves allowed to visualize the estimated survival for different hypothetical volumes of tumors involving cluster III, showing a clear "dose-dependency" of tumor volume on shortening OS. The estimated median OS was 551, 434, and 357 days for hypothetical tumor volumes of 67 cc

Downloaded from aacrjournals.org/clincancerres/article-pdf/32/11/2230/3796381/ccr-25-4419.pdf by DKFZ - German Cancer Research Center, m.krumbach@dkfz.de on 28 October 2026

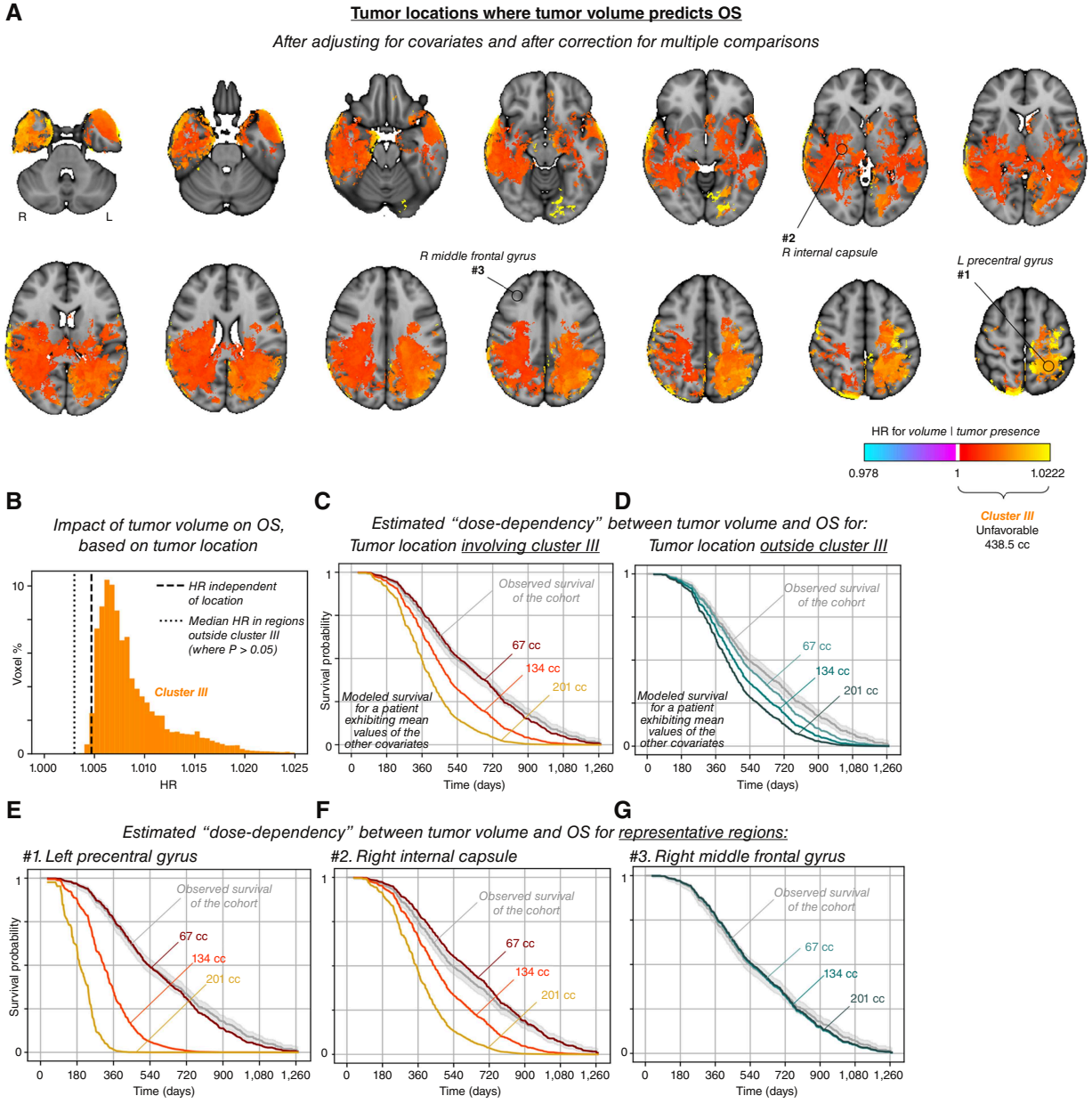


Figure 3.

Impact of tumor volume on survival for different voxel-wise tumor locations (*volume | tumor presence* in *model 4*). In numerous bilateral hemispheric tumor locations (cluster III, orange-yellow in **A**), a larger tumor volume was associated with shorter survival, whereas it was not a significant predictor in other regions, such as bilateral anterior frontal areas. Notably, the effect size of tumor volume in cluster III (orange in **B**) was larger than tumor volume independent of tumor location (dashed line in **B**) and larger than tumor volume in regions outside cluster III (dotted line in **B**). This difference can be also visualized by comparing modeled survival curves for different hypothetical tumor volumes with localization in cluster III (**C**) and outside cluster III (**D**) and by comparing specific representative regions belonging to cluster III (**E** and **F**) and outside cluster III (**G**). cc, cubic centimeters; L, left; R, right.

(mean of the cohort), 134 cc (2 × mean), and 201 cc (3 × mean), respectively (**Fig. 3C**). Conversely, in regions outside cluster III, the effect of tumor volume was less important and was considered not statistically significant in the model (modeled median OS: 503 days for 67 cc, 459 days for 134 cc, and 420 days for 201 cc, **Fig. 3D**). As representative regions, tumor volume showed a clear impact on OS for tumor locations in the left precentral gyrus (region #1, belonging to cluster III, **Fig. 3E**) and in the right internal capsule (region #2, belonging to cluster III, **Fig. 3F**), whereas no dependency was observed in the right middle frontal gyrus (region #3,

Downloaded from aacrjournals.org/clincancerres/article-pdf/32/11/2230/3796381/ccr-25-4419.pdf by DKFZ - German Cancer Research Center, m.krumbach@dkfz.de on 28 October 2026

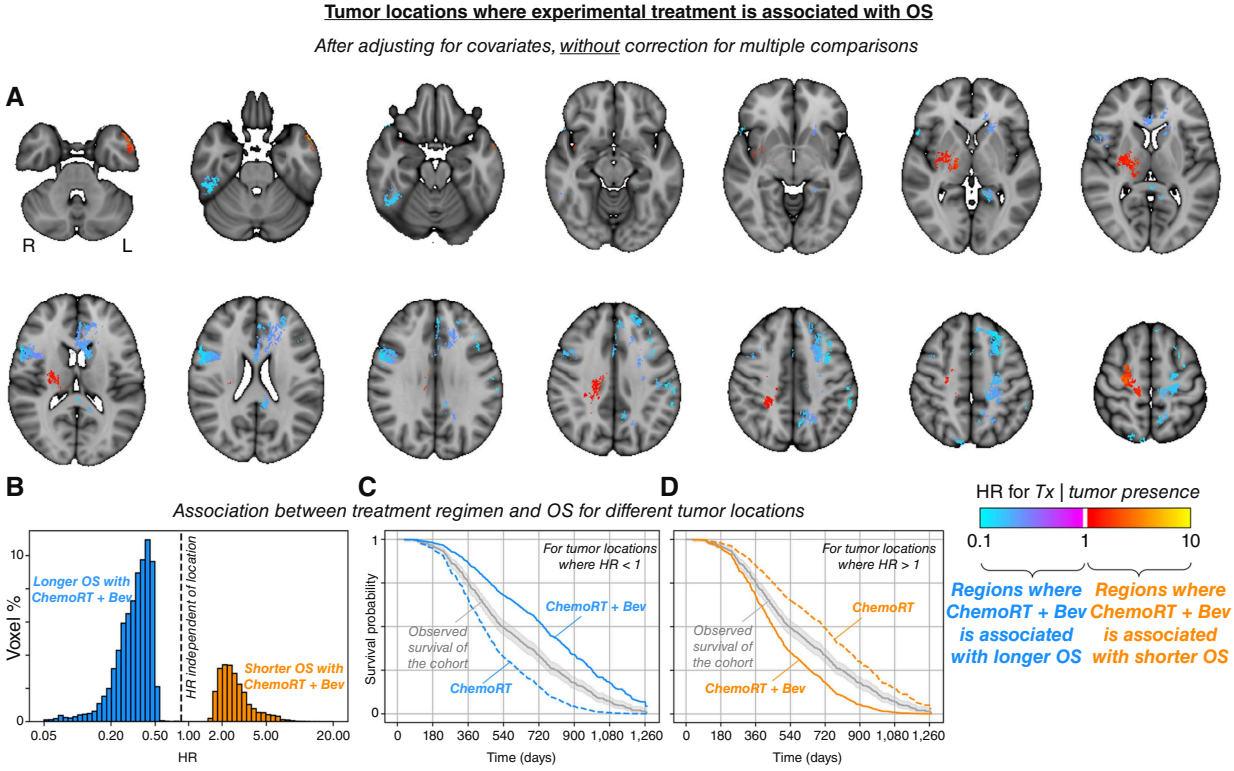


Figure 4.

Impact of treatment arm on survival for different voxel-wise tumor locations (*Tx | tumor presence* in model 5). For tumor location in some superficial cortical regions, mainly in the left hemisphere (blue clusters in **A**), the experimental treatment arm chemoradiation + bevacizumab was associated with longer survival, as also evident from the histogram plots of HR values (blue in **B**) and the modeled survival curves (blue in **C**). Conversely, for tumor location in some right hemisphere regions, including the precentral gyrus and some deep-seated areas (yellow-red clusters in **A**), the experimental treatment arm was associated with shorter survival (orange histograms in **B** and modeled survival curves in **D**). However, these results did not survive the correction for multiple testing and may represent false-positive results. Bev, bevacizumab; ChemoRT, chemoradiation; L, left; R, right.

outside cluster III, **Fig. 3G**), where the modeled survival curves overlap for all hypothetical volumes.

Impact of tumor location on experimental treatment efficacy and survival

Bevacizumab has not shown a survival benefit when compared with placebo, in combination with chemoradiation (3). To disentangle potential interaction effects between tumor location and experimental treatment on OS while accounting for prognostic variables, we expanded the model to include a dedicated interaction term for *tumor presence* and *treatment* (model 5).

The results of SPM (without multiple testing correction) suggest that specific brain tumor locations may be associated with a survival benefit when treated with adjuvant bevacizumab (violet-blue in **Fig. 4**) and others with a survival disadvantage (orange-red in **Fig. 4**). SPM (uncorrected) also showed that experimental treatment was associated with longer survival when the tumor did not localize to brain regions involving the right pyramidal tract and medial lemniscus in the frontoparietal areas and internal capsule, as well as the right thalamus and basal ganglia (purple regions in **Fig. 5**). These statistically uncorrected clusters did not survive the correction for multiple testing and may represent false-positive results. This highlights the importance of including a correction method for multiple testing in voxel-wise studies to control for false-positive results.

Sensitivity analyses and robustness of the results

As a sensitivity analysis, we built a voxel-wise Cox model including both the interaction term of baseline tumor volume and the interaction term of treatment arm, which confirmed that the results of model 4 and model 5 were robust when additional interaction variables were included into a single comprehensive model (model 6; Supplementary Fig. S3). An additional sensitivity analysis verified that the significant clusters (clusters I and II from model 3 and cluster III from model 4) remained significant even when adopting a stricter percentile cutoff in the size-based cluster correction (95th percentile, instead of 90th).

Discussion

Voxel-wise multivariate Cox proportional hazard SPM represents an unbiased data-driven methodology to assess the prognostic value of tumor locations, which represents a substantial advancement compared with more approximative approaches based on qualitative categorizations assigned by the investigator. More importantly, in this work, we showcase a flexible framework to perform Cox-SPM with dedicated interaction terms to map the impact of other prognostic variables for different brain regions involved or spared by the tumor. This approach represents an innovative tool for accurate prognostication, as mapping prognostic variables onto specific brain

Downloaded from aacrjournals.org/clincancerres/article-pdf/32/11/2230/3796381/ccr-25-4419.pdf by DKFZ - German Cancer Research Center, m.krumbach@dkfz.de on 28 October 2026

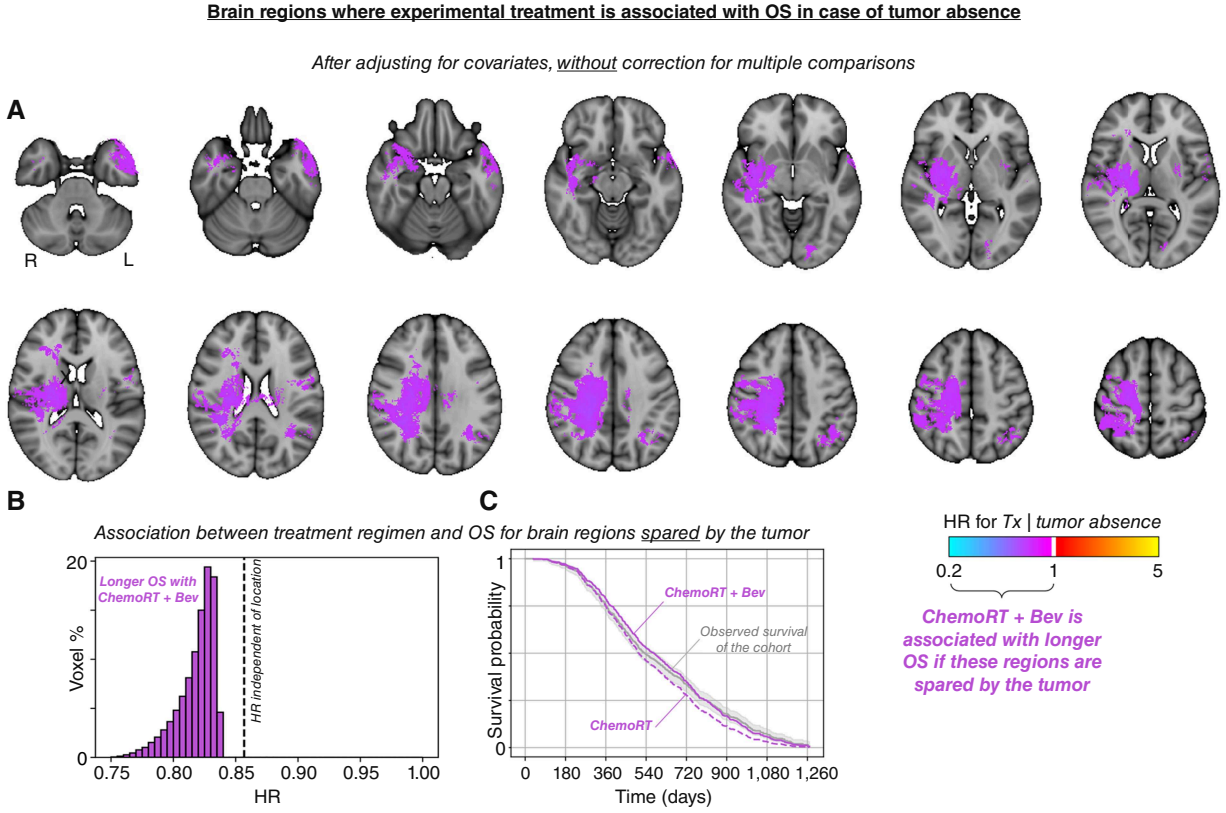


Figure 5.

Impact of treatment arm on survival for regions spared by tumor location (*Tx | tumor absence* in model 5). The experimental treatment arm chemoradiation + bevacizumab was associated with longer survival when tumors spared specific brain regions, particularly a large cluster that involves the right pyramidal tract territory and right-hemisphere deep-seated areas (purple in **A**), also shown with the histogram plots of HR values (purple in **B**) and with the modeled survival curves (purple in **C**). However, these results did not survive the correction for multiple testing and may represent false-positive results. Bev, bevacizumab; ChemoRT, chemoradiation; L, left; R, right.

regions may reveal a location-dependent impact, as we show for pretreatment tumor volume, with potential relevance for the understanding of the disease and with clinical implications for risk stratification and clinical management. Additionally, the models can also encode information about the treatment regimen, along with dedicated interaction variables, to investigate whether specific tumor locations may benefit from specific therapeutic agents. Although the results of this analysis were not significant after multiple testing correction for the specific treatment used in this clinical trial, this overall approach represents a valuable tool for *post hoc* analyses of clinical trial data to reveal potential relationships between treatment efficacy and tumor locations. This research direction is particularly appealing because of the inherent genetic and epigenetic differences in lesions arising in different brain regions (23, 63–66), which may be linked to a different susceptibility to specific experimental treatments. Finally, within the overall framework, we also present a methodology to generate modeled survival probability curves for patients with lesion locations in specific brain regions while setting the other covariates to any desired hypothetical value. Such survival curves greatly improve the overall understanding of the model results, allowing for a clear visualization of the estimated survival, as well as median OS computation, for any given variable in any brain region.

Potential model variations

This framework can be considered as a flexible tool that can be adapted to investigate the interplay of brain lesion locations in modulating the association between any variables of interest and any time-to-event outcome. Three main aspects can be object of variations in voxel-wise Cox-SPM: the lesion segmentations, the covariates and interaction terms, and the outcome. As an alternative to evaluating whole presurgical lesion, segmentations may outline specific tumor components (e.g., contrast-enhancing, metabolically active, or hyperperfused) at different time points (e.g., pre- or postsurgical, postradiation, or at recurrence). For instance, there is a growing interest in evaluating the survival impact of postsurgical contrast-enhancing residual, the volume of which is a strong predictor of OS (50). Cox-SPM may be adapted by using postsurgical residual segmentations for the variable *tumor presence*, which would yield maps reflecting residual locations associated with survival. However, this approach would require a very large sample size, as residuals are small and SPM requires a certain minimal number of observations per voxel. A different approach to incorporating postsurgical residuals is to simply adjust for the residual contrast-enhancing volume while maintaining whole-lesion presurgical segmentations (exploratory analyses in Supplementary Table S2; Supplementary Fig. S4). The resulting brain maps (Supplementary Fig. S4) display the presurgical tumor involvement regions that are

Downloaded from aacrjournals.org/clincancerres/article-pdf/32/11/2230/3796381/ccr-25-4419.pdf by DKFZ - German Cancer Research Center, m.krumbach@dkfz.de on 28 October 2026

significantly associated with survival independent of postsurgical residual volume (but not accounting for the residual location). Similarly, other covariates of interest may be included in variations of the voxel-wise models (e.g., clinical/neurologic status, comorbidities, prior treatment history for recurrent tumors, and multifocal disease), as well as any desired interaction variables. Notably, some other voxel-wise covariates may be included, other than tumor presence (e.g., radiation dose and advanced imaging metrics). Finally, it is also possible to use a different time-to-event outcome (e.g., progression-free survival, time to neurologic deficit, and time to performance status deterioration). Notably, the applications of this framework extend beyond GBM research, as tumor locations may be substituted with the location of brain metastases or nontumoral lesions (e.g., multiple sclerosis), or even with voxel-wise quantitative metrics extracted from normal-appearing brain in neurology or psychiatry studies, while also adapting covariates and time-to-event outcomes as desired.

Limitations

This cohort of patients was diagnosed and treated between 2009 and 2011; therefore, the IDH mutation status of the studied lesions is unknown. However, it is likely that almost the entirety of these cases represent IDH wild-type gliomas, as <1% of the AVAglio cohort was estimated as potentially "secondary GBM" by the pathologists (67) and as <4% of histopathology-defined GBM are IDH-mutant based on epidemiologic data (1). Clinical trial cohorts may not be fully representative of the patient population (Supplementary Table S3). The presurgical tumor location was based on the segmentation of the tumor regions and surgical cavity on postsurgical T_2w FLAIR images, which was an inevitable approximation due to the unavailability of presurgical images, acquired off-study before trial enrollment. Although segmentations based on presurgical images may arguably be preferable, they would also bear some limitations, as tumor components with extensive mass effect may displace adjacent brain structures and may be prone to anatomic mismapping after registration (e.g., a right-hemisphere tumor crossing the midline without left-hemisphere tumor involvement may be mismapped onto left-hemisphere MNI regions). Therefore, the use of postsurgical images, less subject to mass effect, should be an acceptable estimate of the approximate anatomic mapping. If presurgical images are used to map tumor locations, the risk of anatomic mismapping may be mitigated using nonlinear registrations (e.g., diffeomorphic) combined with dedicated strategies that maximize anatomic matching, such as cost-function masking (68). More in general, T_2w FLAIR-hyperintense regions are an imperfect surrogate of tumor extension, due to both false-positive areas (i.e., nontumoral FLAIR-positive regions representing edema or postsurgical alterations) and false-negative areas (i.e., FLAIR-negative regions with microscopic tumor infiltration). Investigators should be aware of the biological significance of the segmentation of choice, when interpreting SPM-Cox results. Multiple testing correction used a size-based cluster correction, which may potentially label as false positive some real biological effects observed in smaller clusters (47). However, multiple testing correction for voxel-wise analyses is currently a complex statistical problem, for which each suggested approach has its own biases (47). Finally, our results from one single cohort cannot be considered conclusive for the ultimate identification of prognostic tumor locations and of brain regions where tumor volume is prognostic, and our SPM results should mainly be interpreted as a display of this novel statistical workflow.

Conclusion

This study showcases a novel framework to implement quantitative statistical maps of brain tumor locations associated with survival outcomes while also mapping the effect of treatment regimens and prognostic variables for tumors located in different brain regions. This represents a robust methodologic tool to investigate the prognostic value of brain tumor locations, reveal novel location-dependent effects of prognostic variables, and potentially interrogate the location-dependent effectiveness of specific treatment schemes. The application of this framework has relevant implications in risk stratification, clinical management, and potentially patient selection for dedicated treatments.

Data Availability

Source code and documentation for voxel-wise Cox models with and without interaction variables, along with the code to calculate the *P* value for combined coefficients, can be found at: https://github.com/BTIL-UCLA/COX_open. The patient data from the AVAglio trial can be made available upon request, pending approval from the sponsor, and under data sharing agreements. Requests for all data can be directed to the corresponding author.

Authors' Disclosures

L.E. Abrey reports other support from Roche during the conduct of the study. B. Simmons reports employment with Roche/Genentech during this clinical trial. O. Chinot reports personal fees and nonfinancial support from Roche during the conduct of the study. W. Wick reports grants and personal fees from Servier outside the submitted work. T.F. Cloughesy reports personal fees and other support from Katmai Pharmaceuticals, 501c3 Global Coalition for Adaptive Research, and Jazz Pharmaceuticals and personal fees from Novo Holdings, Third Rock Ventures, Symbio Generrics, Boxer Capital, Mundipharma, Tango Therapeutics, BlueRock Therapeutics, Vida Ventures, Lisata Therapeutics, Stemline Therapeutics, Novartis, Roche, SonALAsense, Sagimet Biosciences, Clinical Care Options, IDEOlogy Health, Servier, Jubilant, ImmVira, Gan & Lee Pharmaceuticals, BrainStorm Cell Therapeutics, Sapience Therapeutics, INOVIO Pharmaceuticals, Vigeo Therapeutics, DNAtrix, TYME Inc., SDP, Kintara Therapeutics, Bayer, Merck, Boehringer Ingelheim, VBL Therapeutics, Amgen, Kiyatec, AbbVie, VBI Vaccines, Deciphera Pharmaceuticals, Agios Pharmaceuticals, Novocure, Imvax, Exelixis, Medscape, and Pathos outside the submitted work, as well as a patent for UC case No(s). 2003-172, 2017-973, 2019-630, 2020-446, 2021-014, 2021-059, 2021-060, 2021-083, 2021-091, 2021-232, 2023-067-1, UCLA 2023-049-1, and 2023-118 issued and licensed to Katmai Pharmaceuticals. B.M. Ellingson reports personal fees from Global Coalition for Adaptive Research, Imaging Endpoints, Jazz Pharmaceuticals, Katmai Pharmaceuticals, Medicenna, Voiant Clinical, Medscape, LLC, Merit CRO, Monteris, Neosoma, Nuvation Bio, Sapience Therapeutics, Servier Pharmaceuticals, Telix Pharmaceuticals, and Third Rock Ventures and grants and personal fees from Siemens outside the submitted work. No disclosures were reported by the other authors.

Authors' Contributions

F. Sanvito: Conceptualization, data curation, software, formal analysis, validation, investigation, visualization, methodology, writing–original draft, writing–review and editing. **C. Raymond:** Data curation, software, writing–review and editing. **D. Telesca:** Formal analysis, supervision, methodology, writing–review and editing. **J. Yao:** Supervision, visualization, writing–review and editing. **L.E. Abrey:** Resources, data curation, project administration, writing–review and editing. **J. Garcia:** Resources, data curation, funding acquisition, writing–review and editing. **B. Simmons:** Data curation, writing–review and editing. **O. Chinot:** Data curation, project administration, writing–review and editing. **F. Saran:** Resources, data curation, project administration, writing–review and editing. **R. Nishikawa:** Resources, data curation, investigation, writing–review and editing. **R. Henriksson:** Resources, data curation, investigation, writing–review and editing. **W.P. Mason:** Resources, data curation, writing–review and editing. **W. Wick:** Resources, data curation, writing–review and editing. **T.F. Cloughesy:** Resources, supervision, writing–review and editing. **B.M. Ellingson:** Conceptualization, resources, formal analysis, supervision, funding acquisition, validation, investigation, visualization, methodology, writing–original draft, project administration, writing–review and editing.

Downloaded from aacrjournals.org/clincancerres/article-pdf/32/11/2230/3796381/ccr-25-4419.pdf by DKFZ - German Cancer Research Center, m.krumbach@dkfz.de on 28 October 2026

Acknowledgments

The authors acknowledge the funding support from NIH NCI R01CA270027 (B.M. Ellingson and T.F. Cloughesy), NIH NCI R01CA279984 (B.M. Ellingson), Department of Defense Congressionally Directed Medical Research Programs CA220732 (B.M. Ellingson and T.F. Cloughesy), NIH NCI P50CA211015 (B.M. Ellingson), and Genentech.

Note

Supplementary data for this article are available at Clinical Cancer Research Online (http://clincancerres.aacrjournals.org/).

Received November 18, 2025; revised January 21, 2026; accepted March 11, 2026; posted first March 16, 2026.

References

1. Ostrom QT, Price M, Neff C, Cioffi G, Waite KA, Kruchko C, et al. CBTRUS statistical report: primary brain and other central nervous system tumors diagnosed in the United States in 2016-2020. Neuro Oncol 2023;25:iv1–99.
2. Stupp R, Mason WP, Van Den Bent MJ, Weller M, Fisher B, Taphoorn MJB, et al. Radiotherapy plus concomitant and adjuvant temozolomide for glioblastoma. N Engl J Med 2005;352:987–96.
3. Chinot OL, Wick W, Mason W, Henriksson R, Saran F, Nishikawa R, et al. Bevacizumab plus radiotherapy-temozolomide for newly diagnosed glioblastoma. N Engl J Med 2014;370:709–22.
4. Stupp R, Taillibert S, Kanner A, Read W, Steinberg D, Lhermitte B, et al. Effect of tumor-treating fields plus maintenance temozolomide vs maintenance temozolomide alone on survival in patients with glioblastoma: a randomized clinical trial. JAMA 2017;318:2306–16.
5. Cruz Da Silva E, Mercier M-C, Etienne-Selloum N, Dontenwill M, Choulier L. A systematic review of glioblastoma-targeted therapies in phases II, III, IV clinical trials. Cancers (Basel) 2021;13:1795.
6. Lorch M. Re-examining Paul Broca's initial presentation of M. Leborgne: understanding the impetus for brain and language research. Cortex 2011;47:1228–35.
7. Bates E, Wilson SM, Saygin AP, Dick F, Sereno MI, Knight RT, et al Voxel-based lesion–symptom mapping. Nat Neurosci 2003;6:448–50.
8. Meyer S, Kessner SS, Cheng B, Bönstrup M, Schulz R, Hummel FC, et al. Voxel-based lesion-symptom mapping of stroke lesions underlying somatosensory deficits. Neuroimage Clin 2016;10:257–66.
9. Banerjee P, Leu K, Harris RJ, Cloughesy TF, Lai A, Nghiemphu PL, et al. Association between lesion location and language function in adult glioma using voxel-based lesion-symptom mapping. Neuroimage Clin 2015;9:617–24.
10. Shah K, Bhartia V, Biswas C, Sahu A, Shetty PM, Singh V, et al. Tumor location and neurocognitive function-Unravelling the association and identifying relevant anatomical substrates in intra-axial brain tumors. Neurooncol Adv 2024;6:vdae020.
11. Pringle AM, Taylor R, Whittle IR. Anxiety and depression in patients with an intracranial neoplasm before and after tumour surgery. Br J Neurosurg 1999;13:46–51.
12. van Genderen MNG, Belgers V, Niers JM, Douw L, Röttgering JG, Gorter M, et al. Tumor location is associated with mood dysfunction in patients with diffuse glioma. Nat Ment Heal 2024;2:853–64.
13. Satoer D, Vork J, Visch-Brink E, Smits M, Dirven C, Vincent A. Cognitive functioning early after surgery of gliomas in eloquent areas. J Neurosurg 2012;117:831–8.
14. Spena G, D'Agata F, Panciani PP, Buglione di Monale M, Fontanella MM. Supratentorial gliomas in eloquent areas: which parameters can predict functional outcome and extent of resection? PLoS One 2013;8:e80916.
15. Ha SM, Chae EY, Cha JH, Kim HH, Shin HJ, Choi WJ. Association of BRCA mutation types, imaging features, and pathologic findings in patients with breast cancer with BRCA1 and BRCA2 mutations. AJR Am J Roentgenol 2017;209:920–8.
16. Dossus L, Benusiglio PR. Lobular breast cancer: incidence and genetic and non-genetic risk factors. Breast Cancer Res 2015;17:37.
17. Kim T-H, Woo S, Yoon SH, Halpenny DF, Han S, Suh CH. CT characteristics of non-small cell lung cancer with anaplastic lymphoma kinase rearrangement: a systematic review and meta-analysis. AJR Am J Roentgenol 2019;213:1059–72.
18. Mori M, Hayashi H, Fukuda M, Honda S, Kitazaki T, Shigematsu K, et al Clinical and computed tomography characteristics of non-small cell lung cancer with ALK gene rearrangement: comparison with EGFR mutation and ALK/EGFR-negative lung cancer. Thorac Cancer 2019;10:872–9.
19. Okano A, Miyawaki S, Hongo H, Dofuku S, Teranishi Y, Mitsui J, et al. Associations of pathological diagnosis and genetic abnormalities in meningiomas with the embryological origins of the meninges. Sci Rep 2021;11:6987.
20. Fountain DM, Smith MJ, O'Leary C, Pathmanaban ON, Roncaroli F, Bobola N, et al. The spatial phenotype of genotypically distinct meningiomas demonstrate potential implications of the embryology of the meninges. Oncogene 2021;40:875–84.
21. Khuong-Quang DA, Buczkowicz P, Rakopoulos P, Liu XY, Fontebasso AM, Bouffet E, et al. K27M mutation in histone H3.3 defines clinically and biologically distinct subgroups of pediatric diffuse intrinsic pontine gliomas. Acta Neuropathol 2012;124:439–47.
22. Carrillo JA, Lai A, Nghiemphu PL, Kim HJ, Phillips HS, Kharbanda S, et al. Relationship between tumor enhancement, edema, IDH1 mutational status, MGMT promoter methylation, and survival in glioblastoma. AJNR Am J Neuroradiol 2012;33:1349–55.
23. Ellingson BM, Lai A, Harris RJ, Selfridge JM, Yong WH, Das K, et al. Probabilistic radiographic atlas of glioblastoma phenotypes. AJNR Am J Neuroradiol 2013;34:533–40.
24. Makino R, Higa N, Akahane T, Yonezawa H, Uchida H, Takajo T, et al. Alterations in EGFR and PDGFRA are associated with the localization of contrast-enhancing lesions in glioblastoma. Neurooncol Adv 2023;5:vdad110.
25. Schroeder T, Bittrich P, Kuhne JF, Noebel C, Leischner H, Fiehler J, et al. Mapping distribution of brain metastases: does the primary tumor matter? J Neurooncol 2020;147:229–35.
26. Neman J, Franklin M, Madaj Z, Deshpande K, Triche TJ, Sadlik G, et al. Use of predictive spatial modeling to reveal that primary cancers have distinct central nervous system topography patterns of brain metastasis. J Neurosurg 2022;136:88–96.
27. Takeuchi K, Hoshino K. Statistical analysis of factors affecting survival after glioblastoma multiforme. Acta Neurochir (Wien) 1977;37:57–73.
28. Simpson JR, Horton J, Scott C, Curran WJ, Rubin P, Fischbach J, et al. Influence of location and extent of surgical resection on survival of patients with glioblastoma multiforme: results of three consecutive Radiation Therapy Oncology Group (RTOG) clinical trials. Int J Radiat Oncol Biol Phys 1993;26:239–44.
29. Surawicz TS, Davis F, Freels S, Laws ERJ, Menck HR. Brain tumor survival: results from the National Cancer Data Base. J Neurooncol 1998;40:151–60.
30. Fazeny-Dörner B, Wenzel C, Veitl M, Piribauer M, Rössler K, Dieckmann K, et al. Survival and prognostic factors of patients with unresectable glioblastoma multiforme. Anticancer Drugs 2003;14:305–12.
31. Yuile P, Dent O, Cook R, Biggs M, Little N. Survival of glioblastoma patients related to presenting symptoms, brain site and treatment variables. J Clin Neurosci 2006;13:747–51.
32. Mineo J-F, Bordron A, Baroncini M, Ramirez C, Maurage C-A, Blond S, et al. Prognosis factors of survival time in patients with glioblastoma multiforme: a multivariate analysis of 340 patients. Acta Neurochir (Wien) 2007;149:243–5.
33. Nizamutdinov D, Stock EM, Dandashi JA, Vasquez EA, Mao Y, Dayawansa S, et al. Prognostication of survival outcomes in patients diagnosed with glioblastoma. World Neurosurg 2018;109:e67–74.
34. Liu TT, Achrol AS, Mitchell LA, Du WA, Loya JJ, Rodriguez SA, et al. Computational identification of tumor anatomic location associated with survival in 2 large cohorts of human primary glioblastomas. AJNR Am J Neuroradiol 2016;37:621–8.
35. Mistry AM, Hale AT, Chambless LB, Weaver KD, Thompson RC, Ihrie RA. Influence of glioblastoma contact with the lateral ventricle on survival: a meta-analysis. J Neurooncol 2017;131:125–33.
36. Mistry AM, Mummareddy N, Salwi S, Davis LT, Ihrie RA. Glioblastoma distance from the subventricular neural stem cell niche does not correlate with survival. Front Oncol 2020;10:564889.
37. Hertler C, Felsberg J, Gramatzki D, Le Rhun E, Clarke J, Soffietti R, et al. Long-term survival with IDH wildtype glioblastoma: first results from the ETERNITY Brain Tumor Funders' Collaborative Consortium (EORTC 1419). Eur J Cancer 2023;189:112913.

Downloaded from aacrjournals.org/clincancerres/article-pdf/32/11/2230/3796381/ccr-25-4419.pdf by DKFZ - German Cancer Research Center, m.krumbach@dkfz.de on 28 October 2026

38. Blakstad H, Brekke J, Rahman MA, Arnesen VS, Miletic H, Brandal P, et al. Survival in a consecutive series of 467 glioblastoma patients: association with prognostic factors and treatment at recurrence at two independent institutions. PLoS One 2023;18:e0281166.
39. Fekete B, Werlenius K, Tisell M, Pivodic A, Smits A, Jakola AS, et al. What predicts survival in glioblastoma? A population-based study of changes in clinical management and outcome. Front Surg 2023;10:1249366.
40. Friston KJ, Holmes AP, Worsley KJ, Poline J-P, Frith CD, Frackowiak RSJ. Statistical parametric maps in functional imaging: a general linear approach. Hum Brain Mapp 1994;2:189–210.
41. Sörensen A, Blazhenets G, Schiller F, Meyer PT, Frings L; Alzheimer Disease Neuroimaging Initiative. Amyloid biomarkers as predictors of conversion from mild cognitive impairment to Alzheimer's dementia: a comparison of methods. Alzheimers Res Ther 2020;12:155.
42. Green A, Vasquez Osorio E, Aznar MC, McWilliam A, van Herk M. Image based data mining using per-voxel cox regression. Front Oncol 2020;10: 1178.
43. Zhai T, Gu H, Yang Y. Cox regression based modeling of functional connectivity and treatment outcome for relapse prediction and disease subtyping in substance use disorder. Front Neurosci 2021;15:768602.
44. Sanvito F, Kaufmann TJ, Cloughesy TF, Wen PY, Ellingson BM. Standardized brain tumor imaging protocols for clinical trials: current recommendations and tips for integration. Front Radiol 2023;3:1267615.
45. Hagiwara A, Schlossman J, Shabani S, Raymond C, Tatekawa H, Abrey LE, et al. Incidence, molecular characteristics, and imaging features of "clinically-defined pseudoprogression" in newly diagnosed glioblastoma treated with chemoradiation. J Neurooncol 2022;159:509–18.
46. Rosner B. Fundamentals of Biostatistics [Internet]. Boston (MA): Cengage Learning; 2015. Available from: https://books.google.com/books?id=yn4yBgAAQBAJ.
47. Kimberg DY, Coslett HB, Schwartz MF. Power in Voxel-based lesion-symptom mapping. J Cogn Neurosci 2007;19:1067–80.
48. Poline JB, Mazoyer BM. Analysis of individual positron emission tomography activation maps by detection of high signal-to-noise-ratio pixel clusters. J Cereb Blood Flow Metab 1993;13:425–37.
49. Hegi ME, Diserens A-C, Gorlia T, Hamou M-F, de Tribolet N, Weller M, et al MGMT gene silencing and benefit from temozolomide in glioblastoma. N Engl J Med 2005;352:997–1003.
50. Ellingson BM, Abrey LE, Nelson SJ, Kaufmann TJ, Garcia J, Chinot O, et al. Validation of postoperative residual contrast-enhancing tumor volume as an independent prognostic factor for overall survival in newly diagnosed glioblastoma. Neuro Oncol 2018;20:1240–50.
51. Ammirati M, Vick N, Liao YL, Ciric I, Mikhael M. Effect of the extent of surgical resection on survival and quality of life in patients with supratentorial glioblastomas and anaplastic astrocytomas. Neurosurgery 1987; 21:201–6.
52. Bao H, Wang H, Sun Q, Wang Y, Liu H, Liang P, et al. The involvement of brain regions associated with lower KPS and shorter survival time predicts a poor prognosis in glioma. Front Neurol 2023;14:1264322.
53. Bruhn H, Tavelin B, Rosenlund L, Henriksson R. Do presenting symptoms predict treatment decisions and survival in glioblastoma? Real-world data from 1458 patients in the Swedish brain tumor registry. Neurooncol Pract 2024;11:652–9.
54. Sacli-Bilmez B, Firat Z, Topcuoglu OM, Yaltirik K, Ture U, Ozturk-Isik E. Identifying overall survival in 98 glioblastomas using VASARI features at 3T. Clin Imaging 2023;93:86–92.
55. Bao H, Ren P, Yi L, Lv Z, Ding W, Li C, et al. New insights into glioma frequency maps: from genetic and transcriptomic correlate to survival prediction. Int J Cancer 2023;152:998–1012.
56. Fyllingen EH, Bø LE, Reinertsen I, Jakola AS, Sagberg LM, Berntsen EM, et al. Survival of glioblastoma in relation to tumor location: a statistical tumor atlas of a population-based cohort. Acta Neurochir (Wien) 2021;163:1895–905.
57. Gutman DA, Cooper LAD, Hwang SN, Holder CA, Gao J, Aurora TD, et al. MR imaging predictors of molecular profile and survival: multi-institutional study of the TCGA glioblastoma data set. Radiology 2013;267:560–9.
58. Ouyang Z-Q, Zheng G-R, Duan X-R, Zhang X-R, Ke T-F, Bao S-S, et al. Diagnostic accuracy of glioma pseudoprogression identification with positron emission tomography imaging: a systematic review and meta-analysis. Quant Imaging Med Surg 2023;13:4943–59.
59. Wangaryattawanich P, Hatami M, Wang J, Thomas G, Flanders A, Kirby J, et al. Multicenter imaging outcomes study of the Cancer Genome Atlas glioblastoma patient cohort: imaging predictors of overall and progression-free survival. Neuro Oncol 2015;17:1525–37.
60. Palpan Flores A, Vivancos Sanchez C, Roda JM, Cerdán S, Barrios AJ, Utrilla C, et al. Assessment of pre-operative measurements of tumor size by MRI methods as survival predictors in wild type IDH glioblastoma. Front Oncol 2020;10:1662.
61. Wood JR, Green SB, Shapiro WR. The prognostic importance of tumor size in malignant gliomas: a computed tomographic scan study by the Brain Tumor Cooperative Group. J Clin Oncol 1988;6:338–43.
62. Lacroix M, Abi-Said D, Fourney DR, Gokaslan ZL, Shi W, DeMonte F, et al. A multivariate analysis of 416 patients with glioblastoma multiforme: prognosis, extent of resection, and survival. J Neurosurg 2001;95:190–8.
63. Ellingson BM, Cloughesy TF, Pope WB, Zaw TM, Phillips H, Lalezari S, et al. Anatomic localization of O6-methylguanine DNA methyltransferase (MGMT) promoter methylated and unmethylated tumors: a radiographic study in 358 de novo human glioblastomas. Neuroimage 2012;59:908–16.
64. Incekara F, van der Voort SR, Dubbink HJ, Atmodimedjo PN, Nandoe Tewarie R, Lycklama G, et al. Topographical mapping of 436 newly diagnosed IDH wildtype glioblastoma with vs. without MGMT promoter methylation. Front Oncol 2020;10:596.
65. Wang Y, Fan X, Zhang C, Zhang T, Peng X, Qian T, et al. Identifying radiographic specificity for phosphatase and tensin homolog and epidermal growth factor receptor changes: a quantitative analysis of glioblastomas. Neuroradiology 2014;56:1113–20.
66. Mu L, Wang Y, Wang Y, Zhang H, Shang D, Tan F, et al. Tumor location and survival outcomes in adult patients with supratentorial glioblastoma by levels of toll-like receptor 9 expression. World Neurosurg 2017;97:279–83.
67. Louis DN, Perry A, Wesseling P, Brat DJ, Cree IA, Figarella-Branger D, et al. The 2021 WHO classification of tumors of the central nervous system: a summary. Neuro Oncol 2021;23:1231–51.
68. Prasanna P, Mitra J, Beig N, Nayate A, Patel J, Ghose S, et al. Mass Effect Deformation Heterogeneity (MEDH) on Gadolinium-contrast T1-weighted MRI is associated with decreased survival in patients with right cerebral hemisphere Glioblastoma: a feasibility study. Sci Rep 2019;9:1145.

Downloaded from aacrjournals.org/clincancerres/article-pdf/32/11/2230/3796381/ccr-25-4419.pdf by DKFZ - German Cancer Research Center, m.krumbach@dkfz.de on 28 October 2026